Wind and Structures, *Vol. 29, No. 6 (2019) 471-488*
DOI: https://doi.org/10.12989/was.2019.29.6.471

Field measurement and CFD simulation of wind pressures on rectangular attic

Yongbo Peng[1a], Weijie Zhao[2b] and Xiaoqiu Ai*[3]

[1]*State Key Laboratory of Disaster Reduction in Civil Engineering & Shanghai Institute of Disaster Prevention and Relief, Tongji University, 1239 Siping Road, Shanghai 200092, P.R. China*
[2]*College of Civil Engineering, Tongji University, 1239 Siping Road, Shanghai 200092, P.R. China*
[3]*Shanghai Institute of Disaster Prevention and Relief, Tongji University, 1239 Siping Road, Shanghai 200092, P.R. China*

(Received November 27, 2018, Revised May 17, 2019, Accepted May 30, 2019)

Abstract. Wind pressure is a critical argument for the wind-resistant design of structures. The attempt, however, to explore the wind pressure field on buildings still encounters challenges though a large body of researches utilizing wind tunnel tests and wind field simulations were carried out, due to the difficulty in logical treatments on the scale effect and the modeling error. The full-scale measurement has not yet received sufficient attention. By performing a field measurement, the present paper systematically addresses wind pressures on the rectangular attic of a double-tower building. The spatial and temporal correlations among wind speed and wind pressures at measured points are discussed. In order to better understand the wind pressure distribution on the attic facades and its relationship against the approaching flow, a full-scale CFD simulation on the similar rectangular attic is conducted as well. Comparative studies between wind pressure coefficients and those provided in wind-load codes are carried out. It is revealed that in the case of wind attack angle being zero, the wind pressure coefficient of the cross-wind facades exposes remarkable variations along both horizontal and vertical directions; while the wind pressure coefficient of the windward facade remains stable along horizontal direction but exposes remarkable variations along vertical direction. The pattern of wind pressure coefficients, however, is not properly described in the existing wind-load codes.

Keywords: wind pressure; wind speed; spatial and temporal correlations; field measurement; CFD simulation; rectangular attic

1. Introduction

Definition of wind loads is viewed as a critical step in the design of flexible structures, especially in today's inevitable trend towards increasing spans and heights of bridges, buildings, power transmission or wind turbine towers, etc. Since these slender structures usually exhibit low natural frequencies, wind loads thus become the dominant load in most situations. Besides, the natural wind is essentially a nonstationary random process even in the case of normal climate conditions. Wind loads applied on flexible structures are thus of stochastic nature, which results in a difficulty for structural engineers to logically define the dominant load. Many efforts of studying wind characteristics have been paid for addressing this issue in recent years.

The wind engineering community primarily embraces three means when studying the wind characteristics, i.e., field measurements, wind tunnel tests and computational fluid dynamics (CFD) simulations. As a most robust and convincing means, the field measurement has been adopted for investigating wind speed and wind pressure against flexible structures. Li *et al*. performed full-scale measurements on two tall-buildings with thirty floors and seventy floors, respectively, and discussed the probabilistic nature of wind speed (Li *et al.* 1998). Maruyama *et al.* studied the distribution of maximum cross-correlation coefficients of pressures based on the field measurement data from a 2.4 m cube (Maruyama *et al*. 2008). Fu et al. conducted an experiment on a 432 m high building during Typhoon 'Megi', and addressed the probability density distribution, turbulence intensity, gust factor and power spectral density of wind speed (Fu *et al.* 2012). Richards and Hoxey measured the wind pressure on a 6m cube and presented a set of integrated pressure coefficients, including the mean, the standard deviation, the maximum and minimum pressure coefficients (Richards and Hoxey 2012). Zhao *et al.* built up understanding of fluctuating wind pressure distribution around cooling towers by conducting full-scale measurements (Zhao *et al*. 2017). Unfortunately, however, due to high requirements of time and investments, the wind data obtained from field measurement are still too deficient to have a full understanding of the wind characteristics, especially for the measurement data of complicated wind field in urban central areas. Besides, the existing wind field studies using field measurements mostly focus on investigation of nature wind, and seldom focus on the wind pressure. As a consequence, the relationship between wind speed and wind pressure has rarely been studied. Moreover, the spatial correlation of wind pressures at different spatial points was not paid sufficient attention, though it is a critical factor in calculating wind loads on spatial structures for gust response analysis. (Zeng *et al.*

*Corresponding author, Assistant Professor
E-mail: aixiaoqiu@tongji.edu.cn
[a] Professor
E-mail: pengyongbo@tongji.edu.cn
[b] Master Student
E-mail: zhaoweijie93@126.com

ISSN: 1226-6116 (Print), 1598-6225 (Online)

Fig. 1 Geographical location and landscape of double-tower building at campus of Tongji University in Shanghai China

2017, Peng *et al*. 2018b).

Based on the similarity law, wind tunnel tests simulate the wind field around a building or bridge by creating a reduced-scale model in an artificial wind tunnel and applying certain boundary conditions on it. The wind tunnel test is a preferable means since it can effectively reduce the hours and expenses costed during wind characteristics studies. Moreover, the wind field conditions can be expediently controlled (Ko *et al*. 2005). Despite all the advantages, however, of wind tunnel tests mentioned above, this means is incapable of bypassing the scale effects between the tested models and prototype structures, as well as the wind field around them.

CFD techniques in simulating wind field around buildings have gained huge progress during the past few decades with the development of both computer technologies and numerical simulation methods. It has a benefit of readily offering flow data such as velocity, pressure and other physical quantities of interest over the entire computational domain by virtue of relatively low requirements. Huang et al. studied mean and fluctuating wind pressures on a standard tall building using both the Reynolds-averaged Navier–Stokes (RANS) and the large eddy simulation (LES) methods (Huang *et al*. 2007). Kose and Dick compared the results of CFD simulation of mean wind pressures on a cubical building using RANS, hybrid RANS/LES and LES schemes (Köse and Dick 2010). Tominaga explored wind field around different building forms using CFD techniques (Tominaga 2015). Nevertheless, to produce accurate results, CFD techniques still remain open on solving complicated wind field problems involving impingement, separation, reattachment and circulation of turbulent eddies. As a matter of fact, the turbulence models and relevant parameters adopted in CFD simulations need to be modified in real time so as to create consistent results with the data obtained from field measurements or wind tunnel tests (Blocken 2014, Blocken *et al*. 2016).

This paper presents an investigation of wind pressures on the rectangular attic of a double-tower building by performing a field measurement. The nature wind in terms of the turbulence intensity and turbulence integral length scale, power spectral density and statistical histogram of the approaching flow is explored as well. The power spectral density and statistical histogram of wind pressures are addressed. Considering that the spatial and temporal variations of wind field are critical for gust response analysis of structures, the correlation analyses among wind speed and wind pressures are also included. A full-scale CFD simulation of the wind field around the rectangular attic is also conducted to further reveal the wind pressure distribution on the entire facades of the rectangular attic. For calibrating purposes, comparative studies between wind pressure coefficients derived from CFD simulations and those provided in wind-load codes are carried out. The remaining sections in the paper are arranged as follows. Section 2 describes the details of local site and facilities for field measurement. The nature wind involving wind speed, temperature, turbulence intensity and turbulence integral length scale is addressed. Power spectral densities, statistical histograms, spatial and temporal correlations of wind speed and wind pressures are discussed in Section 3. Section 4 presents full-scale CFD simulations and comparative studies against the existing wind-load codes for revealing the pattern of wind pressure coefficients. Influences of wind attack angles on wind pressure coefficients are also investigated. The concluding remarks are addressed in Section 5.

2. Field measurement

2.1 Wind observation facilities

The field measurement system was built up on the rectangular attic of a double-tower building at the campus of Tongji University in Shanghai China, as shown in Fig. 1. This double-tower building is located in the urban center area and surrounded by trees and dense buildings with different heights. The dimensions of the double-tower building are 68.7 m in length, 48.0 m in width and 50.0 m from the ground to the roof and then 6.0 m from the roof to the top of attic. The dimensions of the rectangular attic on the roof are 8.4 m in length, 8.4 m in width and 6.0 m in height. Besides, there are surrounding parapets with height of about 1.8 m above the roof surface of the building. The shortest distance between the parapets and the external wall of the attic is only around 6.0 m.

For the purpose to investigate the characteristics of local wind velocity and wind pressure on external walls of buildings, a set of wind observation facilities was placed on the top of the building, including one anemometer (type RM Young 05103), one temperature probe (type 109), and three wind pressure transducers (type CYG1721). It is seen from Fig. 2 that the three wind pressure transducers, labelled CH1, CH2 and CH3, are adhered centrally on the three

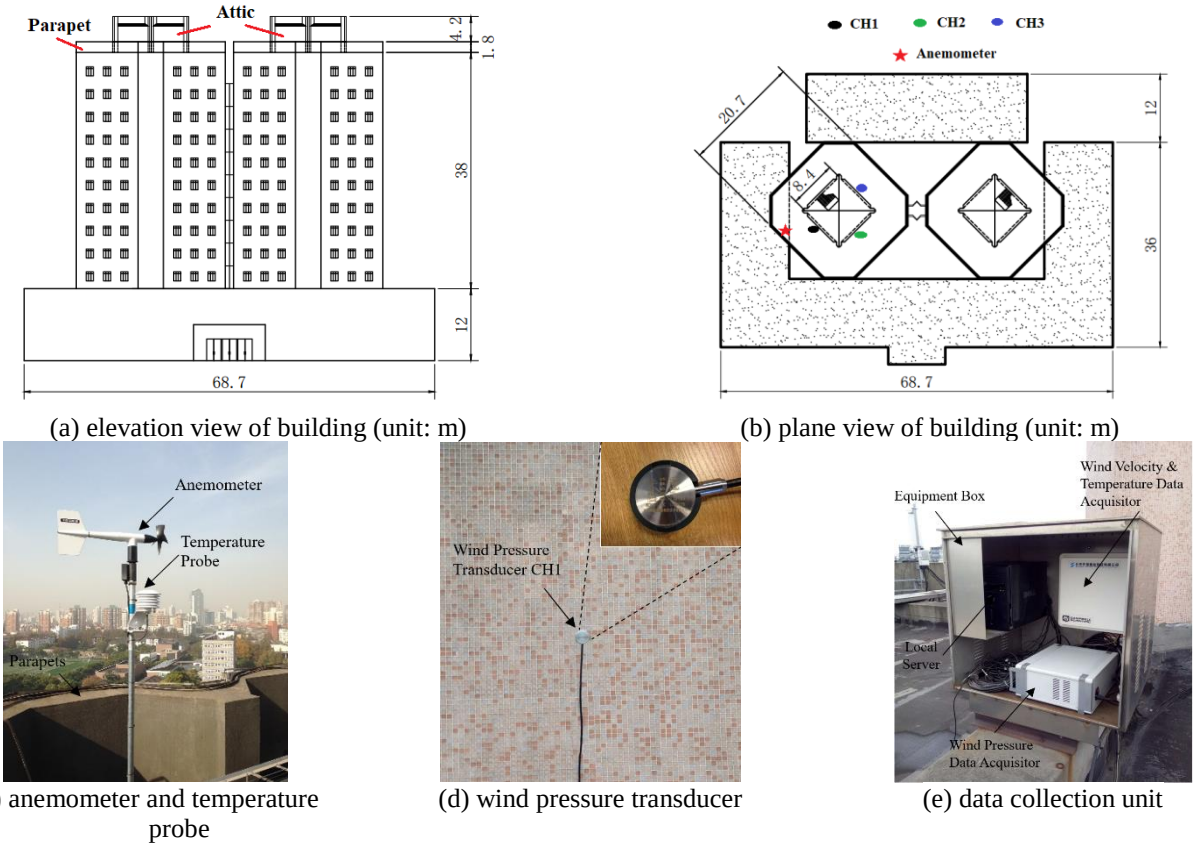

(a) elevation view of building (unit: m)

(b) plane view of building (unit: m)

(c) anemometer and temperature probe

(d) wind pressure transducer

(e) data collection unit

Fig. 2 Layout of wind observation facilities applied in field measurement system

external walls of the attic and lifted 2.5 m from the building roof. The anemometer is set at 2.5 m as well above the building roof, and 5.5 m apart from the external wall where the wind pressure transducer CH1 is placed. The temperature probe is deployed together with the anemometer. A set of data acquisition unit and power supply is packaged in an equipment box which is placed on the building roof. The sampling frequencies of the three kinds of wind observation facilities are set to 1Hz.

2.2 Nature wind

The data of wind speed and wind pressures was collected on 11th February, 2014. In order to attain an understanding of the nature wind, the daily measured data is first averaged on each velocity readings with time spans of 10 min to obtain mean wind speeds over the 24 hours, as shown in Fig. 3(a). The turbulence intensity denoting the fluctuating degree of wind speed is then derived; see Fig. 3(b), which is defined as the ratio between the standard deviation of fluctuating wind speed and the mean wind speed. In order to reveal the variation of wind direction, the wind rose diagram derived from wind data collected in the 24 hours is presented in Fig. 3(c). One might recognize from Fig. 1 that the 10-min mean wind speeds are in the range of 1.0 m/s-2.8 m/s; the turbulence intensity varies from 30% to 80%; and the wind mainly comes from the northwest direction. The data of wind speed and wind pressure collected on 11th February, 2014 is of concern since the wind velocity in this period exhibits a relatively large amplitude and a more stable direction. In addition, as for the high turbulence intensity, it owes to (i) the double-tower building is located at an urban center area with dense buildings resulting in a large surface roughness length; (ii) the turbulence intensity tends to be high when the wind speed is in a low level (Ren *et al*. 2018).

Temperature is a critical argument related to air density and viscosity. In order to keep track of the temperature field along wind flows simultaneously, a complete time series of temperature consistent with the wind data was collected. Fig. 4 shows the mean temperatures on time spans of 10 min through 00:00 a.m. to 24:00 p.m. The temperature ranges from about -3℃ to 3℃, which is quite typical in the winter season in Shanghai.

The fluctuating wind is usually viewed as the result of the superposition of periodical eddy fluctuations with different scales existing in the natural wind, i.e., the fluctuating wind shares some similarities with traveling wave. Given that U and f denotes the mean wind speed and the eddy frequency, respectively, the ratio between U and f would naturally be the wave length (namely length scale) of eddies. Turbulence integral length scale is defined as the average of eddy length scales during a certain time span in turbulence flow. Based on Taylor's hypothesis, the definition of turbulence integral length scale is given by (Peng *et al*. 2018b)

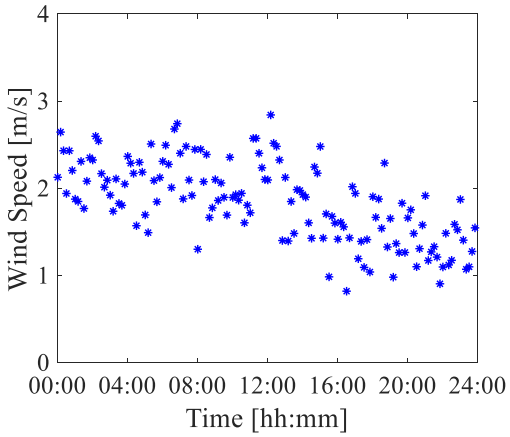

(a) mean wind speeds

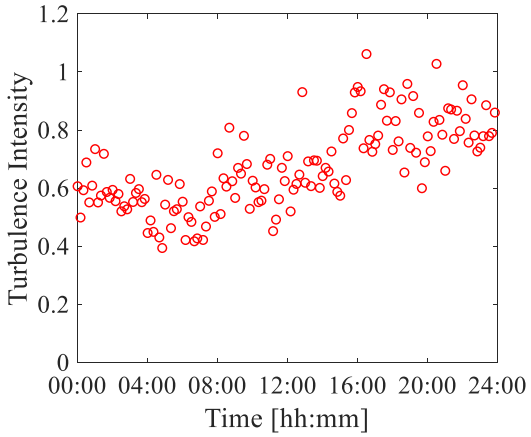

(b) turbulence intensities

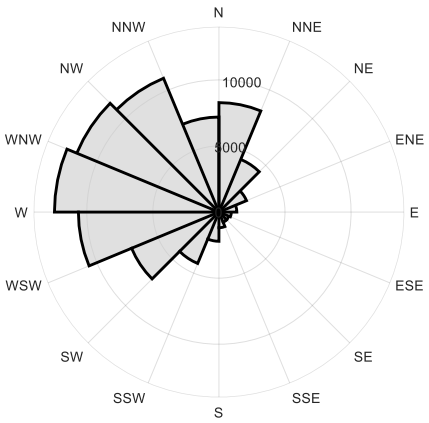

(c) wind rose diagram

Fig. 3 Nature wind of local monitoring site on building roof.

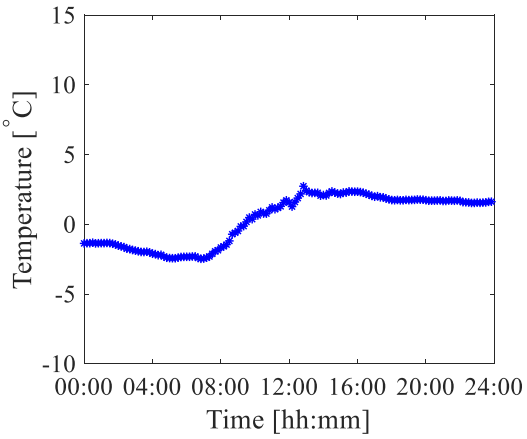

Fig. 4 Mean temperatures of local monitoring site on building roof

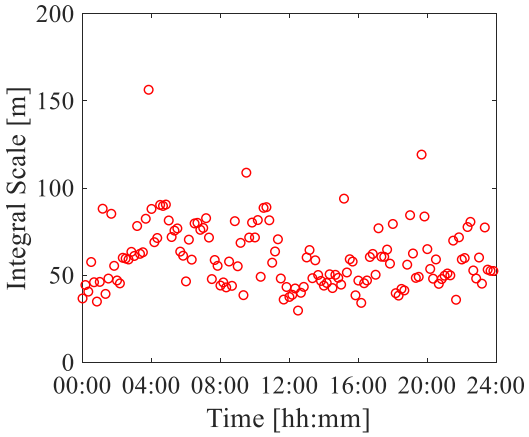

Fig. 5 Along-wind turbulence integral length scales of local monitoring site on building roof

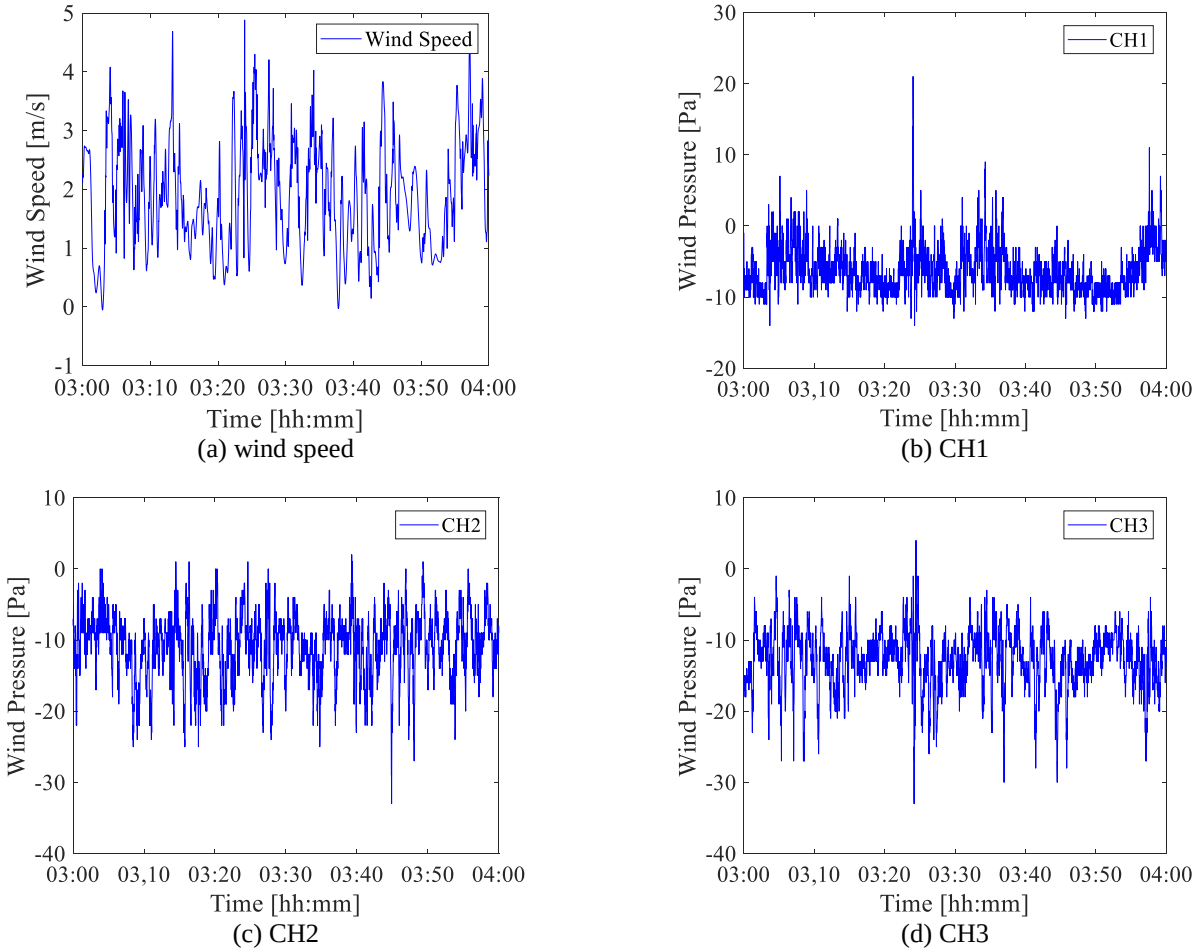

Fig. 6 Time series of wind speed and wind pressures on position CH1, CH2 and CH3 of external walls of attic collected through 03:00 a.m. to 04:00 a.m. on 11th February, 2014

$$L_u = U(z)\int_0^{\infty} \frac{u(t)u(t+\tau)}{\sigma_u^2}\mathrm{d}\tau \qquad (1)$$

where $U(z)$ denotes the mean wind speed at the specific elevation z; $u(t)$ denotes the fluctuating wind speed; σ_u denotes the standard deviation of the fluctuating wind speed; and τ denotes the time lag between fluctuating wind speeds.

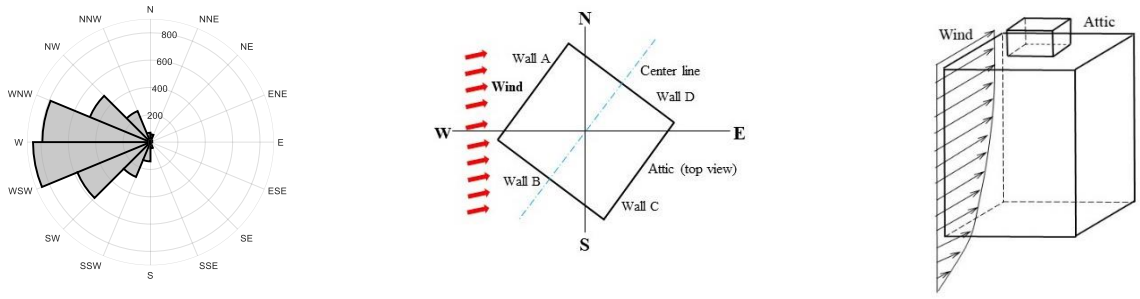

(a) wind rose diagram (b) azimuth of attic

Fig. 7 Schematic diagrams of wind direction and azimuth of attic collected through 03:00 a.m. to 04:00 a.m. on 11th February, 2014

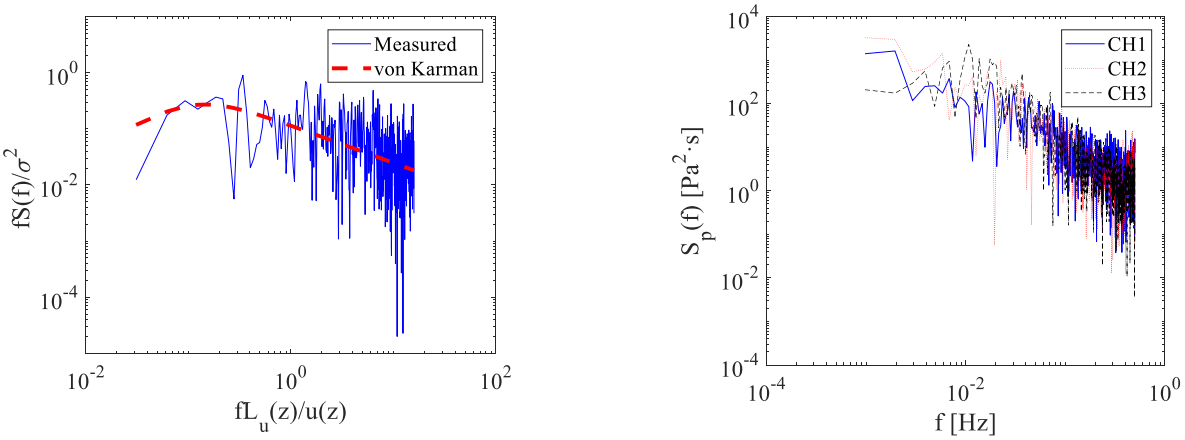

(a) power spectral densities of wind speed (b) power spectral densities of wind pressures

Fig. 8 Power spectral densities of wind speed and wind pressures of sample series in time span through 03:00 a.m. to 03:10 a.m

Fig. 5 presents the along-wind turbulence integral length scales at the elevation of 52.5 m. The average turbulence integral scale of the fluctuating wind speed is 60.3 m, and the coefficient of variation is 30.7%. One might understand that the smaller turbulence integral length scale owes to the low mean wind speed and the large surface roughness length involved in the present studies.

2.3 Wind pressures

Fig. 6 shows time series of the wind speed and wind pressures on the external walls of the attic collected through 03:00 a.m. to 04:00 a.m. on 11th February, 2014, including the data derived from wind pressure transducers CH1, CH2 and CH3. The time interval selected in this hour is based on the wind condition, of which the wind direction was relatively stable and the wind speed was relatively larger. In order to conduct a qualitative analysis, schematic diagrams that contain the information of wind direction and the azimuth of the attic are drawn in Fig. 7. It is seen that for most seconds during 03:00 a.m. to 04:00 a.m., the wind blows from the east to the west. This wind direction and the azimuth of the building result in a nearly 45° skew intersection between the approaching flow and the external walls A and B of the attic; see Fig. 7(b). It is thus indicated that the external walls A and D are in combination of windward and cross-wind facades, while the external walls B and C are in combination of cross-wind and leeward facades. According to the data of wind pressures, the hourly mean wind pressures from CH1, CH2 and CH3 are -6.22 Pa, -10.87 Pa and -12.76 Pa, respectively, which is reasonable in qualitative sense that follows the rule of wind pressure distribution on square shape building (Abdusemed and Ahuja 2016).

3. Wind spectrum analysis

3.1 Power spectral densities

Power spectrum density of fluctuating wind speed depicts the energy distribution of fluctuating wind over frequency domain. Based on the Kolmogrove's hypotheses, a collection of wind spectra have been proposed in the past few decades (Kármán 1948, Davenport 1961, Kaimal *et al.* 1972, Simiu 1974). As one of the most widely-used wind spectra in wind engineering community, the von Karman spectrum is employed in this study, of which the function

Table 1 Skewness and kurtosis of fluctuating wind speed and fluctuating wind pressure

Statistical moments	Fluctuating wind speed	Fluctuating wind pressure CH1	Fluctuating wind pressure CH2	Fluctuating wind pressure CH3	Gaussian distribution
Skewness	0.4332	1.3736	-0.5506	-0.6344	0
Kurtosis	2.6734	7.4491	3.3439	4.1827	3

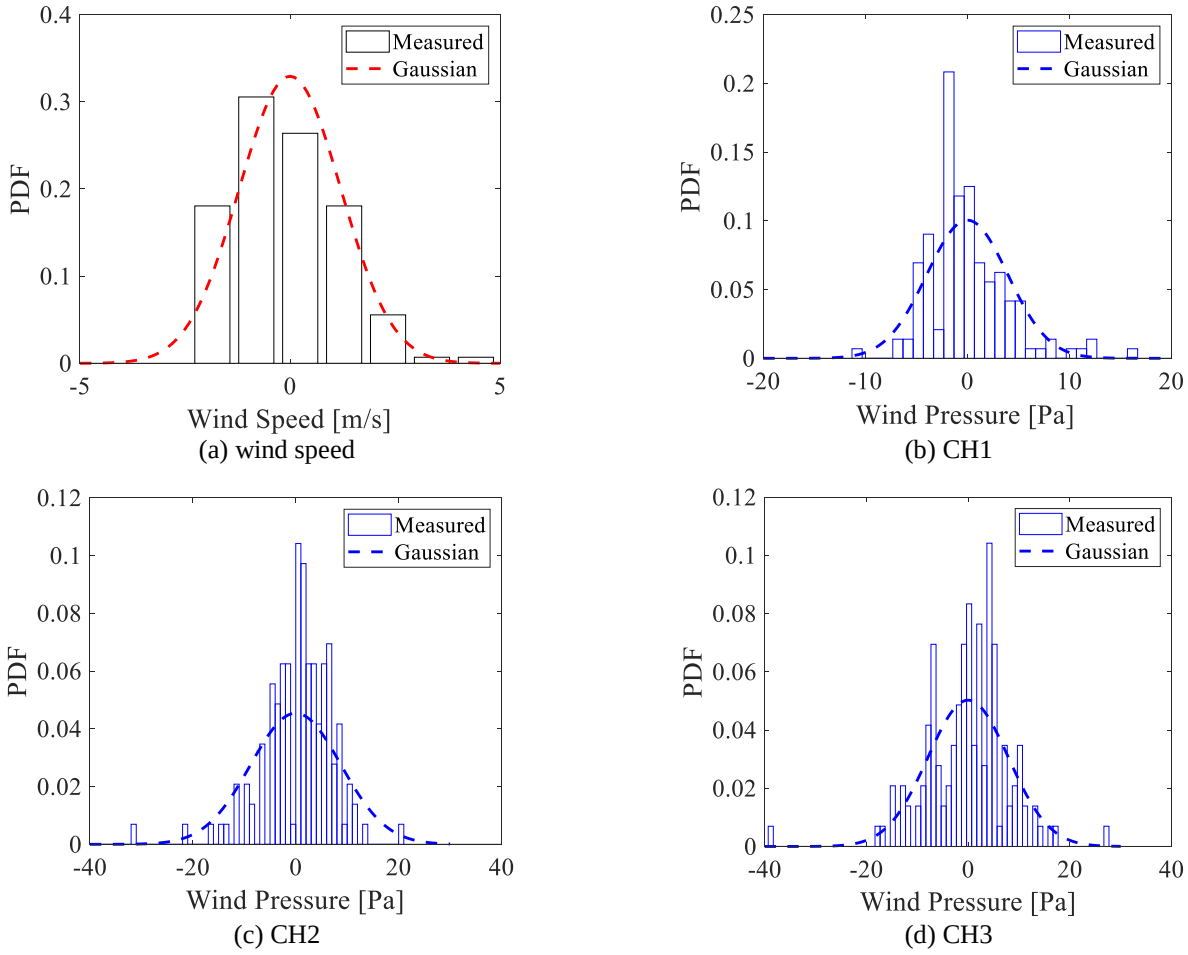

Fig. 9 Uniformed histograms and Gaussian distributions of fluctuating wind speed and fluctuating wind pressures in time span through 03:00 a.m. to 04:00 a.m

expression is given as (Peng *et al*. 2018b)

$$\frac{fS_u(f)}{\sigma_u^2}=\frac{4\left(fL_u/U(z)\right)}{\left[1+70.8\left(fL_u/U(z)\right)^2\right]^{5/6}} \tag{2}$$

where f denotes the frequency of fluctuating wind in Hz; L_u denotes the average turbulence integral length scale; $U(z)$ denotes the average longitudinal wind speed at the specific altitude of z; $S_u(f)$ denotes the power spectral density of fluctuating wind speed over the frequency domain.

To explore the consistency between the measured data and power spectral density, a sample series in the time span through 03:00 a.m. to 03:10 a.m. is investigated. Fig. 8(a) shows the power spectral density of the sample series. For comparative study, the von Karman spectrum is also presented. It is seen that the wind spectrum of field measurement and the von Karman spectrum show a good consistency in both low and high frequency domains. Spectral analysis on the measured wind pressure is conducted as well using similar methods. Fig. 8(b) shows the power spectral densities of sample series of wind pressures collected from CH1, CH2 and CH3 in the time span through 03:00 a.m. to 03:10 a.m. It is revealed that the power spectral densities of wind pressures on different external walls of the attic share a similar distribution over both low and high frequency domains. Considering that wind direction is about 270 degrees during the selected period, CH1 is in the windward region, while CH2 and CH3 are in the wake region. The reason why all three spectra of

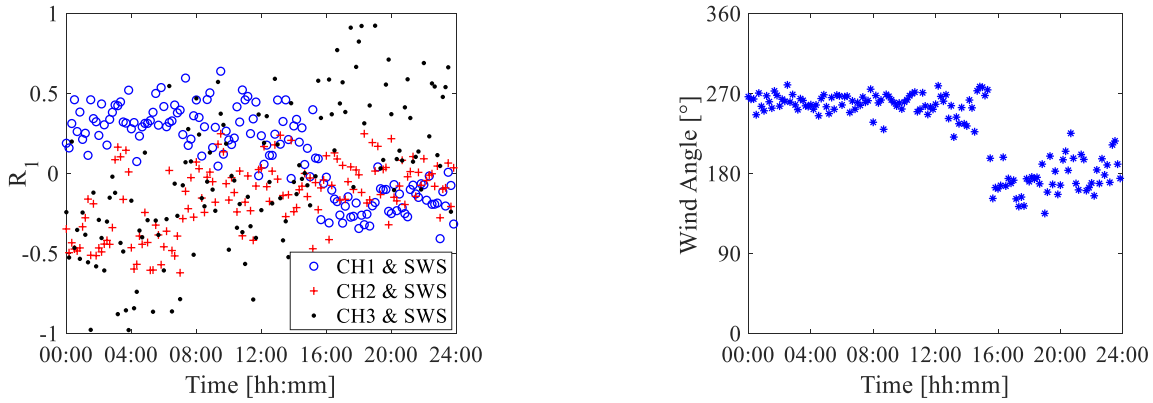

(a) correlation coefficients (b) wind angle in degree

Fig. 10 Correlation coefficients between square of mean wind speed (SWS) and mean wind pressures with time spans of 10 min, and wind angle in degree

wind pressure show similarity remains unclear, and a possibility is the main building's effect on the wind field around the attic.

3.2 Statistical histograms

In the analysis of randomly wind-induced response and reliability assessment of structures, the fluctuating wind speed is generally simulated as a zero-mean Gaussian process by virtue of spectral representation methods (Shinozuka and Deodatis 1996, Hu *et al.* 2010, Ai *et al.* 2016, Song *et al*. 2018, Liu *et al*. 2018). However, this is not rigorously applicable when the atmosphere turbulence is disturbed by near-ground objectives such as urban landscape. Fig. 9 presents the uniformed histograms and Gaussian distributions of fluctuating wind speed and fluctuating wind pressures in the time span through 03:00 a.m. to 04:00 a.m., where the Gaussian distributions exhibit same statistical parameters as the uniformed histograms. It is seen that the statistical distribution of fluctuating wind speed exposes a similarity with the Gaussian distribution; while those of fluctuating wind pressures expose an obvious difference from the Gaussian distribution. High-order moments, i.e., skewness and kurtosis, of fluctuating wind speed and fluctuating wind pressures are shown in Table 1.

One might recognize that neither the fluctuating wind speed nor the fluctuating wind pressure submits to Gaussian distribution rigorously. The difference between fluctuating wind speed and Gaussian distribution is not so large that can be regarded as an approximate Gaussian process in wind engineering community (Li *et al*. 1998). However, the fluctuating wind pressure should be viewed as a non-Gaussian process.

3.3 Correlation analysis

Correlation coefficient is a metric on the extent of linear relevance between two variables in statistics. In this study, the spatial and temporal correlations among measured wind speed and wind pressures are addressed. The formula of correlation coefficient is defined as (Yan *et al.* 2013)

$$R = \frac{\mathrm{cov}(X,Y)}{\sigma_X \sigma_Y} \tag{3}$$

where X and Y are two variables that denote measured data of wind speed or wind pressure; σ_X, σ_Y denote the standard deviation of X and Y, respectively; cov(X,Y) denotes the covariance of X and Y.

The approaching flow collected at the position of the anemometer is approximately viewed as the input velocity on the external walls A and B of the attic. In order to address the functional correlation between the measured wind speed and wind pressure, the wind data collected from the entire day is analysed. The correlation coefficients of the square of wind speed and wind pressure are calculated using Eq. (3), where X denotes the square of mean of measured velocity readings with time spans of 10 min; see $X=U^2$ (z)/1630 (ASCE 2010), where Y denotes the mean of measured pressure readings with time spans of 10 min from the wind pressure transducers CH1, CH2 and CH3. Considering that the functional correlation is also dependent on the wind angle, the mean of wind angle readings with time spans of 10 min is investigated as well; as shown in Fig. 10. It is seen that the correlation coefficient R_1 between the approaching flow and the wind pressures collected from CH1 and CH2 varies mostly in range of -0.5 to 0.5, which reveals a weak correlation; while the correlation coefficient R_1 between the approaching flow and the wind pressure collected from CH3 varies in range of -1.0 to 1.0, revealing a strong correlation. Besides, the correlation coefficient between CH1 and approaching flow varies from the positive to negative after around 4:00 p.m., and that between CH3 and approaching flow varies from the negative to positive at almost the same time. This can be inferred from the sudden change of wind direction from about 270 degrees to approximately 180 degrees; see Fig. 10(b). Meanwhile, one might recognize that the change of wind direction does not

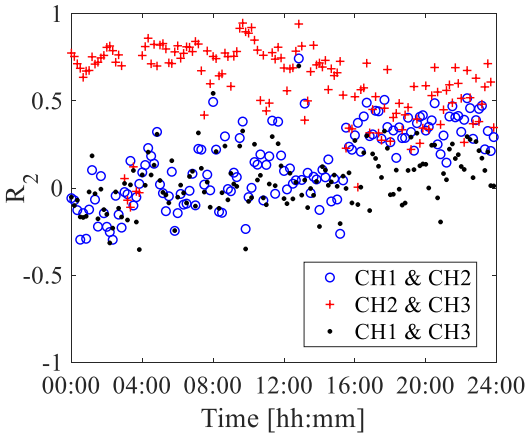

Fig. 11 Correlation coefficients between mean wind pressures with time spans of 10 min

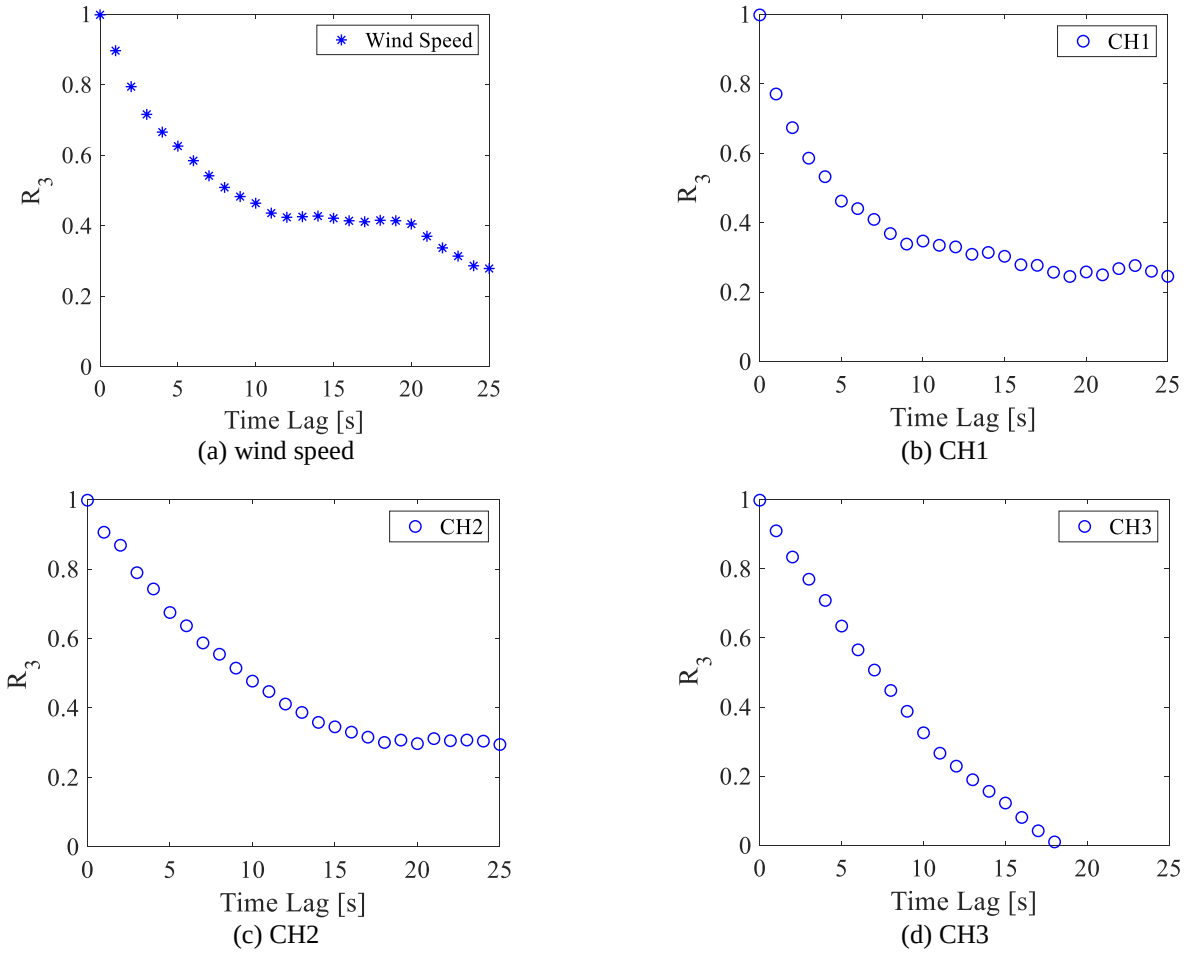

Fig. 12 Autocorrelation coefficients of wind speed and wind pressures against time lag in time span through 03:00:00 a.m. to 03:10:25 a.m

affect so seriously on the correlation coefficient between CH2 and approaching flow since the position of the wind pressure transducer always towards the windward regardless of the wind angle 270 or 180 degrees.

The spatial correlation of wind pressures collected from the transducers CH1, CH2 and CH3 are investigated as well. It is seen from Fig. 11 that the correlation coefficient R_2 between the wind pressure data collected from CH1 and CH2, and that collected from CH1 and CH3 both vary in

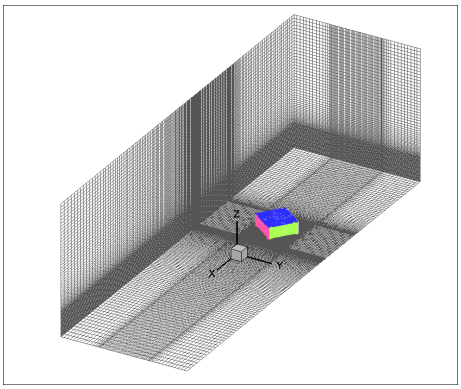

(a) flow domain

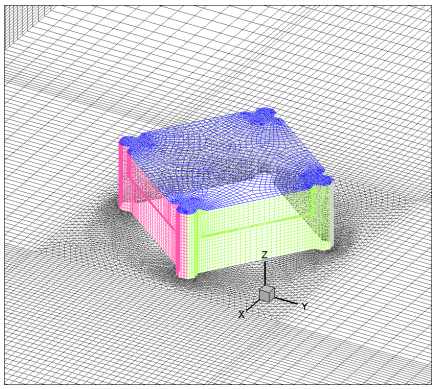

(b) meshed full-scale rectangular attic model

Fig. 13 Mesh configurations of flow domain and full-scale rectangular attic model

range of -0.5 to 0.5; while that collected from CH2 and CH3 varies between 0 and 1. The wind pressures on the positions of external walls with CH1 and CH2, and on the positions of external walls with CH1 and CH3 thus have a poor spatial correlation; while the wind pressures on the positions of external walls with CH2 and CH3 has a moderate spatial correlation. As mentioned previously, the wind blows from the west to the east, and the particular azimuth of the attic leads to the external walls adhered with transducers CH2 and CH3 arising to be a combination of crosswind and leeward facades.

For the analysis of temporal correlation of wind data, the time series of wind speed and wind pressures collected through 03:00:00 a.m. to 03:10:25 a.m. are considered. The time lag between *X* and *Y* is set as ranging from 0 s to 25 s. For instance, in the calculation of correlation coefficient of CH1 with time lag 10 s, *X* represents the wind pressure CH1 in the time interval between 03:00:00 a.m. and 03:10:00 a.m., and *Y* represents the wind pressure CH1 in the interval between 03:00:10 a.m. to 03:10:10 a.m. The correlation coefficients against the time lag are presented in Fig. 12. It is readily seen that, as a whole, the autocorrelation coefficients R_3 of wind speed and wind pressures on different external walls become smaller increasingly with the time lag. One might recognize that the autocorrelation coefficients of the wind speed and the wind pressures derived from CH1, CH2 have a similarity since the anemometer and the transducers CH1, CH2 locate at an almost same windward direction in the time interval with wind direction 270 degrees. However, this similarity is not exposed on the autocorrelation coefficient of the wind pressure derived from CH3 that drops fast to zero before the time lag 20 seconds. Nevertheless, the temporal correlation analysis reveals that the collected wind data is reliable since the measurement accuracies of both the anemometer and transducers are in level of milliseconds.

4. Wind Field Simulations

4.1 CFD simulation setups

Wind pressure coefficient is a critical parameter controlling the wind-resistant design of building structures, which is often determined by wind field simulations and wind tunnel tests in practice. With the purpose of exploring the wind pressure distribution on the external walls of the attic, a full-scale CFD simulation based on steady Reynolds Averaged Navier-Stokes (RANS) equations is carried out. The turbulence model of Realizable $k-\varepsilon$ is adopted, which has been verified to be accurate on predicting the flow motion associated with separation, reattachment and recirculation (Blocken and Carmeliet 2008, Blocken *et al.* 2012, Montazeri and Blocken 2013, Zheng *et al.* 2016, Mittal *et al.* 2018). The simulation is performed on the platform of Fluent 6.3.26. SIMPLE algorithm is adopted to deal with pressure-velocity coupling, and all variables are treated with second-order discretization schemes.

To ensure a good consistency between results of CFD simulations and full-scale measurement, a 10-sec wind data with both large mean wind speed and small standard deviation of wind angle is picked up for determining the parameters of boundary conditions. All parameters relevant to the boundary conditions of the CFD model are derived from the selected time interval of 10 seconds: the elevation of anemometer H=52.5 m; the horizontal wind speed U_H=4.23 m/s; the mean wind angle θ_m=255.49°; the turbulence intensity I_H=0.122; the integral length scale L_u=34.3 m.

The boundary conditions adopted in this study are defined as the arguments as follows

$$u(z)=\frac{v_f}{\kappa}\ln\left(\frac{z}{z_0}\right) \tag{3}$$

$$k(z)=1.5\left[\bar{U}(z)I(z)\right]^2 \tag{4}$$

$$\varepsilon(z)=0.09^{0.75}\left[k(z)\right]^{1.5}/(\kappa L_u) \tag{5}$$

where $u(z)$ is the mean horizontal wind speed at the elevation of z, $k(z)$ is the turbulence kinetic energy at the elevation of z, $\varepsilon(z)$ is the turbulence dissipation rate at the elevation of z, κ is the von Karman constant (κ=0.4), z_0

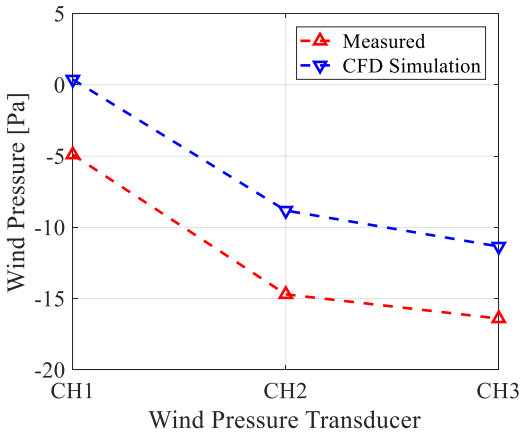

Fig. 14 Comparison of simulated and measured wind pressures at positions adhered with transducers CH1, CH2 and CH3.

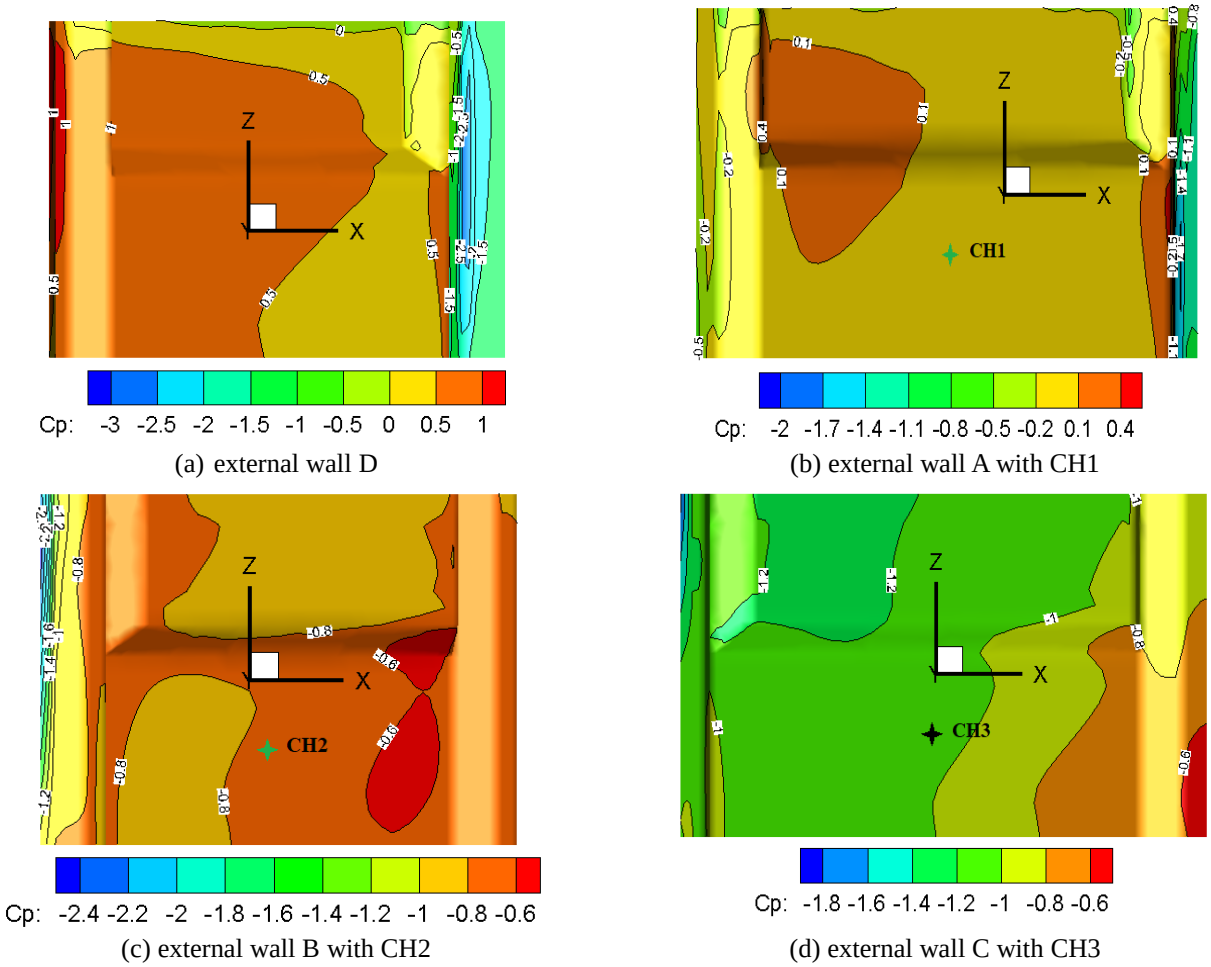

(a) external wall D

(b) external wall A with CH1

(c) external wall B with CH2

(d) external wall C with CH3

Fig. 15 Wind pressure coefficients on external walls of rectangular attic by CFD simulations.

denotes the ground roughness length (z_0=2.0 m), v_f is the friction velocity (v_f=0.502), $I(z)$ is the turbulence intensity of horizontal wind speed at the elevation of z (which refers to the AIJ Recommendations for Loads on Buildings (AIJ-RLB 2004)), L_u denotes the turbulence integral length scale at the elevation of z.

It is mentioned in the previous sections, the full-scale dimensions of the rectangular attic above the roof surface are 8.4 m×8.4 m×6.0 m. However, there are also surrounding parapets with height of about 1.8 m above the roof surface of the building. Thus an 8.4 m×8.4 m×4.2 m model is used, and the flow field around the building is constructed as the practical rules (Franke 2006, Franke *et al.*

Table 2 Comparison of wind pressure coefficients on external walls of model provided by wind-load codes

Wind pressure coefficients	Windward facade (external wall A)	Cross-wind facade (external walls B, D)	Leeward facade (external wall C)
China	+0.8	-0.7	-0.5
USA	+0.8	-0.7	-0.5
Japan	+0.6	-0.7① / -0.4② / (-0.2③)	-0.6
Europe	+0.7	-1.2① / -0.8② / (-0.5③)	-0.3

*in Japan code, the wind pressure coefficient ① assigned on the block with width [0, 0.5*min{4h,b}], the wind pressure coefficient ② assigned on the block with width [0.5*min{4h,b}, 1.5*min{4h,b}], and the wind pressure coefficient ③ assigned on the block with width [1.5*min{4h,b},d].

*in Europe code, the wind pressure coefficient ① assigned on the block with width [0, min{2h,b}/5], the wind pressure coefficient ② assigned on the block with width [min{2h,b}/5, min{2h,b}], and the wind pressure coefficient ③ assigned on the block with width [min{2h,b}, d- min{2h,b}].

* h denotes the height of model; b denotes the windward length of model; d denotes the cross-wind length of model.

2007). Grids of the flow domain are designed to be finer as close to the building, and the total number of volume mesh elements is around 1,220,000. The mesh configurations of the flow domain and the full-scale rectangular attic model are showed in Fig. 13.

4.2 Wind pressure coefficients

Wind pressure coefficient of structures is typically defined as (Clancy 1975, Jendzelovsky *et al*. 2017)

$$C_p = \frac{P - P_{\text{inf}}}{0.5\rho_{\text{inf}} U_{\text{inf}}{}^2} \tag{6}$$

where P denotes static wind pressure at the point of interest; P_{inf} denotes the reference static pressure; ρ_{inf} denotes the air density (ρ_{inf}=1.225 kg/m^3); U_{inf} denotes the reference air velocity. It has been proved that the selection of reference point for P_{inf} and U_{inf} significantly relies upon the buildings with and without balconies (Montazeri and Blocken 2013). In this study, the reference point is determined to the central line of velocity inlet profile at 0.8 m in height where the wind monitor is deployed, and thus P_{inf} =0 Pa, U_{inf}=4.23 m/s.

The numerical accuracy of CFD simulations is first examined through comparative studies against the measured wind pressures collected from the transducers CH1, CH2 and CH3. It is seen from Fig. 14 that the wind pressures at the three observation points are all negative values, which indicates a wind suction effect. The simulated wind pressures, meanwhile, exhibit smaller values than the measured data with a difference around 5 Pa. However, the variations of simulated and measured wind pressures from CH1 to CH3 show a consistent trend. Considering the complexity inherent in the natural wind field and the simplicity on the measures adopted by CFD simulations, the numerical prediction results are still acceptable for qualitative analysis.

The wind pressure coefficients distributed on the external walls A, B, C and D of the rectangular attic are shown in Fig. 15, where positive and negative values indicate the wind push effect and wind suction effect, respectively. It is seen from the contour of wind pressure coefficients on the external wall adhered with CH1 appears to zero in the central area, but exposes a drastic change from +0.4 to -2.0 at the wall corner. Wind pressure coefficients on the external walls adhered with CH2 and CH3 show stable negative wind pressures: the former varies from -0.6 to -2.4 and the latter varies from -0.6 to -1.8. The results are similar to the findings in previous experimental investigations (Abdusemed and Ahuja 2016), where the wind pressure coefficient distributions on external walls of a square shape tall building under wind attack angle 45° were explored by wind tunnel tests.

4.3 Comparative studies against wind-load codes

Rectangular section and flat roof underlie a widely-applied configuration of buildings in practice. Wind pressure coefficients with respect to this family of buildings have been well studied and recommended in the wind-load codes for the wind-resistant design of structures. Based on the knowledge in the previous sections, comparative studies between simulated pressure coefficients and recommended pressure coefficients in wind-load codes of China, USA, Japan and Europe are proceeded. The 8.4 m×8.4 m×4.2 m model is investigated here as well, of which the external walls are flatted as a typical building with rectangular section and flat roof.

The relevant provisions in the involved wind-load codes are first addressed, including the *Load Code for the Design of Building Structures* by China Academy of Building Research (CABR 2012), the *Minimum Design Loads for Buildings and Other Structures* by American Society of Civil Engineers (ASCE 2010), the *Recommendations for Loads on Buildings* by Architectural Institute of Japan (AIJ-RLB 2004), and the *Eurocode 1: Actions on Structures* by European Committee of Standardization (CEN 2004). The wind pressure coefficients on external walls of the model provided by the wind-load codes are shown in Table 2.

It is seen from Table 2 that for the 8.4 m×8.4 m×4.2 m model, China and USA codes offer a relatively conservative provision on the wind pressure coefficient of windward facade compared with Japan and Europe codes; the provision on the leeward facade offered in Europe code is more radical; and the wind pressure coefficient on the cross-wind facades shows a typical difference from the wind-load codes. China and USA codes suggest a same

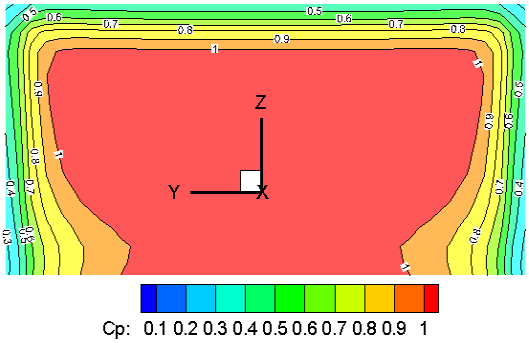

(a) windward facade (external wall A)

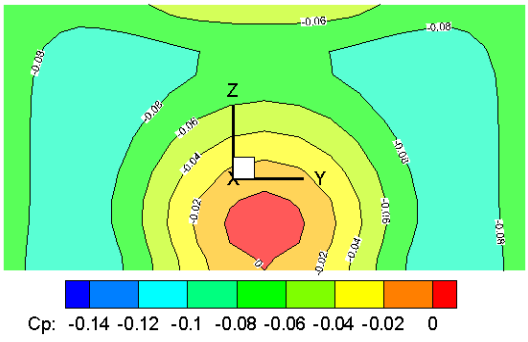

(b) leeward façade (external wall C)

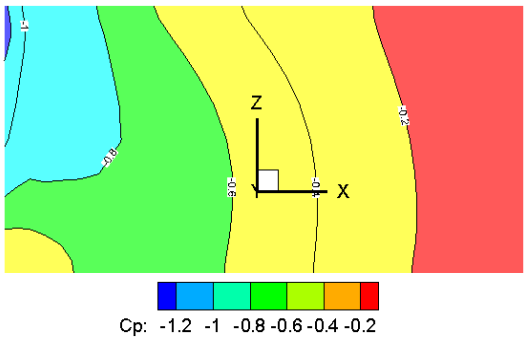

(c) cross-wind façade (external wall B)

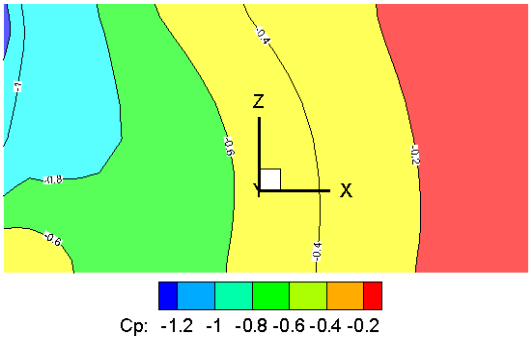

(d) cross-wind façade (external wall D)

Fig. 16 Wind pressure coefficients on facades with wind attack angle 0°

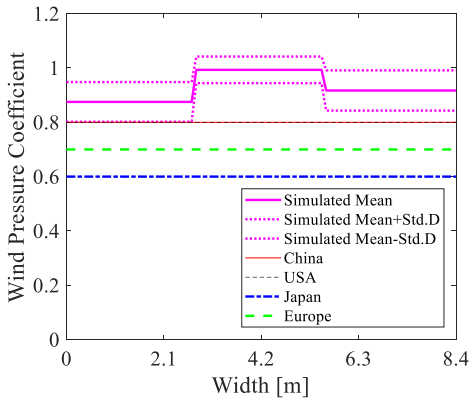

(a) windward facade (external wall A)

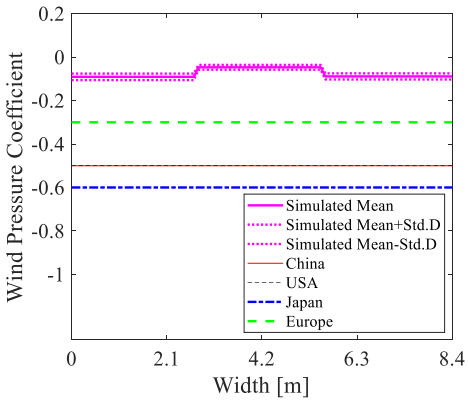

(b) leeward façade (external wall C)

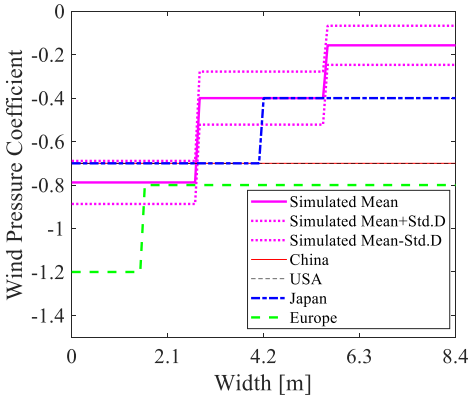

(c) cross-wind façade (external walls B and D)

Fig. 17 Wind pressure coefficients by CFD simulation and in provisions of wind-loads codes

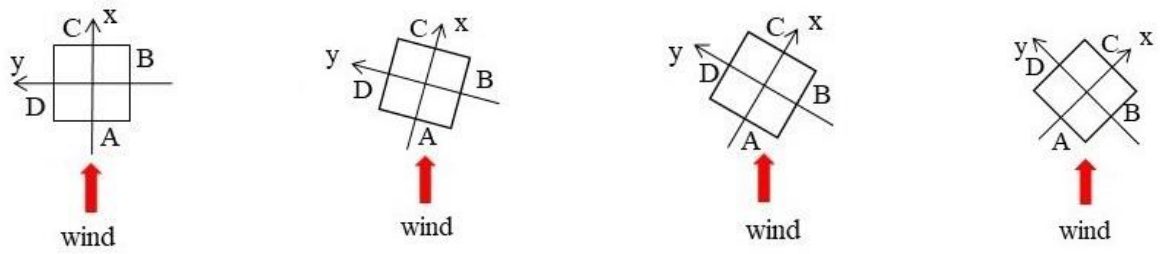

(a) 0° (b) 15° (c) 30° (d) 45°

Fig. 18 Schematic of four cases with wind attack angles towards the attic (top view).

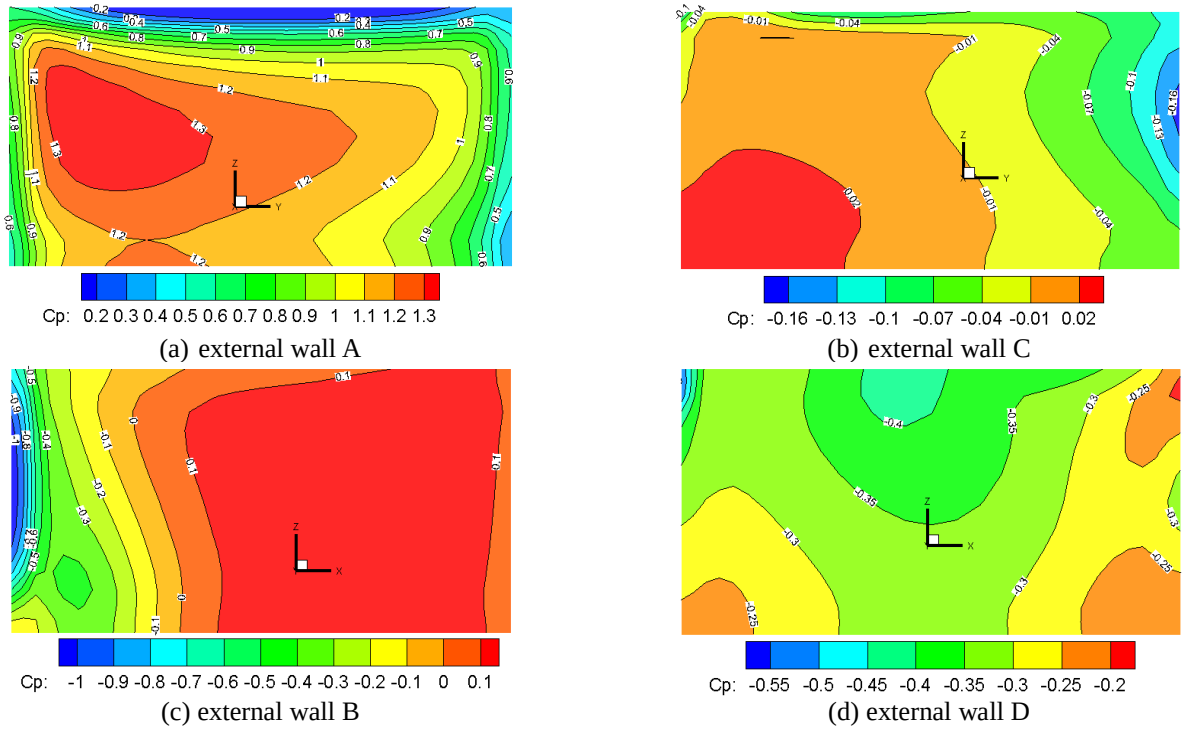

(a) external wall A (b) external wall C

(c) external wall B (d) external wall D

Fig. 19 Pressure coefficient distribution on external walls with wind attack angle 15°

pressure coefficient on the entire cross-wind facades, i.e., -0.7. However, Japan and Europe codes recommend a three-block pressure coefficient on the cross-wind facades, and each block is assigned a pressure coefficient as the principles below Table 2. Besides, the pressure coefficients assigned on the three blocks of the cross-wind facades in Europe code are obviously larger than those in Japan code.

Full-scale CFD simulations on the model are performed to serve as a validation. The turbulence model, boundary conditions and other setups are the same as that detailed in Sections 4.1 and 4.2, except that the wind attack angle is set as 0°. Fig. 16 shows the wind pressure coefficients on different facades, i.e., windward facade (external wall A), leeward facade (external wall C), and cross-wind facades (external walls B and D). It is seen that although the wind pressure coefficients of the all facades vary with the horizontal direction, those of the cross-wind facades arise to be nearly isotropic along the vertical direction; however, those of the windward and leeward facades arise significant variations along the vertical direction. One might recognize that the results of CFD simulations are distinctly different from the provisions from the wind-load codes. A schematic on the differences between the simulated results and the provisions is shown in Fig. 17. It is seen that the simulated results are processed with area-weighted average (Simulated Mean), and their variations (Simulated Mean±Std.D) reveals the fluctuation of wind pressure coefficients along the vertical direction. It is seen that the simulated results approach to the positive compared with the wind-load codes no matter of the windward facades or of the leeward and cross-wind facades. This is due to the numerical error in CFD simulations, as shown in Fig. 14.

It is indicated as well that the block partition on wind pressure coefficients of the cross-wind facades in Japan and Europe codes is reasonable, owing to the fact that the simulated wind pressure coefficients of cross-wind facades significantly vary along the horizontal direction; see Simulated Mean in Fig. 17. While those of windward and

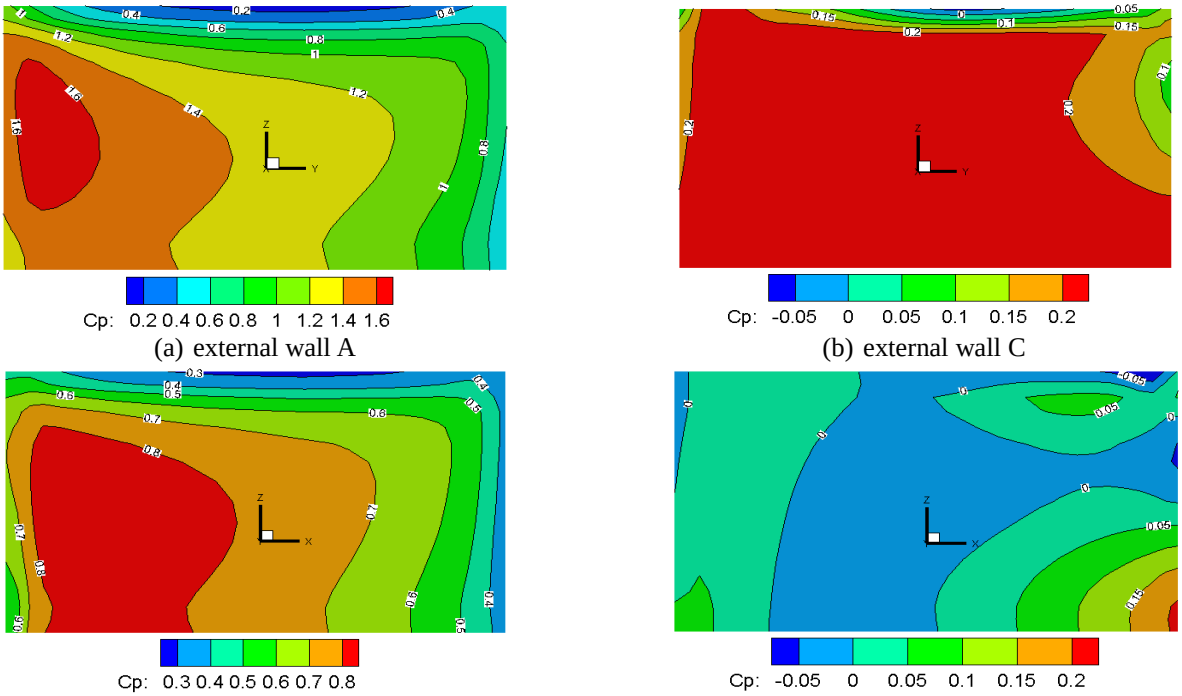

(a) external wall A (b) external wall C

(c) external wall B (d) external wall D

Fig. 20 Pressure coefficient distribution on external walls with wind attack angle 30°

leeward facades slightly vary along the horizontal direction, especially of the leeward façade, which indicates that the wind pressure coefficients of windward and leeward facades could be treated as constant along the horizontal direction, as indicated in the wind-load codes. However, the fluctuation of the simulated wind pressure coefficients of the windward and cross-wind facades appears to be significant, while that of the leeward facades appears to be slight; see Simulated Mean±Std.D in Fig. 17. It is revealed that the variation of wind pressure coefficients of the leeward facades along the vertical direction can be safely ignored, but the windward and cross-wind facades shall contain the anisotropy of wind pressure coefficients along the vertical direction when determining wind loads on structures.

4.4 Influences of wind attack angles

Wind attack angle is a critical factor significantly affecting the wind pressure coefficients distributed on external walls of structures. Generally speaking, the case with wind attack angle 0° is the most unfavorable wind situation for rectangular buildings, as noted in the wind-load code of Europe *Eurocode 1: Actions on Structures* (CEN 2004). While this is not mentioned in the wind-load codes of China, USA, as well as Japan, since no more cases except that with wind attack angle 0° are involved in provisions of these codes. It is revealed, however, in the results of CFD simulations under the cases with the measured and zero wind attack angles that there are some aspects worth of notice concerning the relevance between the wind pressure coefficient distribution and the wind attack angle.

Full-scale CFD simulations using the same setups as detailed in Sections 4.1 and 4.2 are conducted. The simulation model addressed in Section 4.3 is adopted here as well. Four cases with wind attack angles 0°, 15°, 30°and 45°are investigated, respectively. The associated schematic diagrams with wind attack angles towards the attic are shown in Fig. 18. It is seen that when the wind attack angle is just 0°, the external wall A denotes the windward facade; the external walls B and D denote the cross-wind facades; and the external wall C denotes the leeward facade. Nevertheless, the wind situation changes as the variation of wind attack angle, and the external walls will not be the exact windward, cross-wind and leeward facades when the cases with wind attack angles 15°, 30°and 45°are considered. CFD simulation results of the case with wind attack angle 0° are shown in Fig. 16 and have been addressed in Section 4.3. While the simulation results of the remaining three cases are shown in Figs. 19-21. It is seen that for the cases with wind attack angles 15°, 30°and 45°, the wind pressure coefficients of the external wall A are all positive and range from +0.2 to +1.6, which are similar to those of the windward facade under wind attack angle 0° just that the area with maximum wind pressure coefficient becomes smaller and moves towards the left boundary along the rotation between the approaching flow and the attic. For the external wall B, the wind pressure coefficients tend to the positive with the increasing of wind attack angles. While for the external walls C and D, the wind pressure coefficients have no such definite tendency. When the wind attack angle is 45°, a similar orientation between the approaching flow and the azimuth of the attic as the field measurement shown in Fig. 7 is attained. Owing to the seriously geometrical symmetry, the external walls C and D

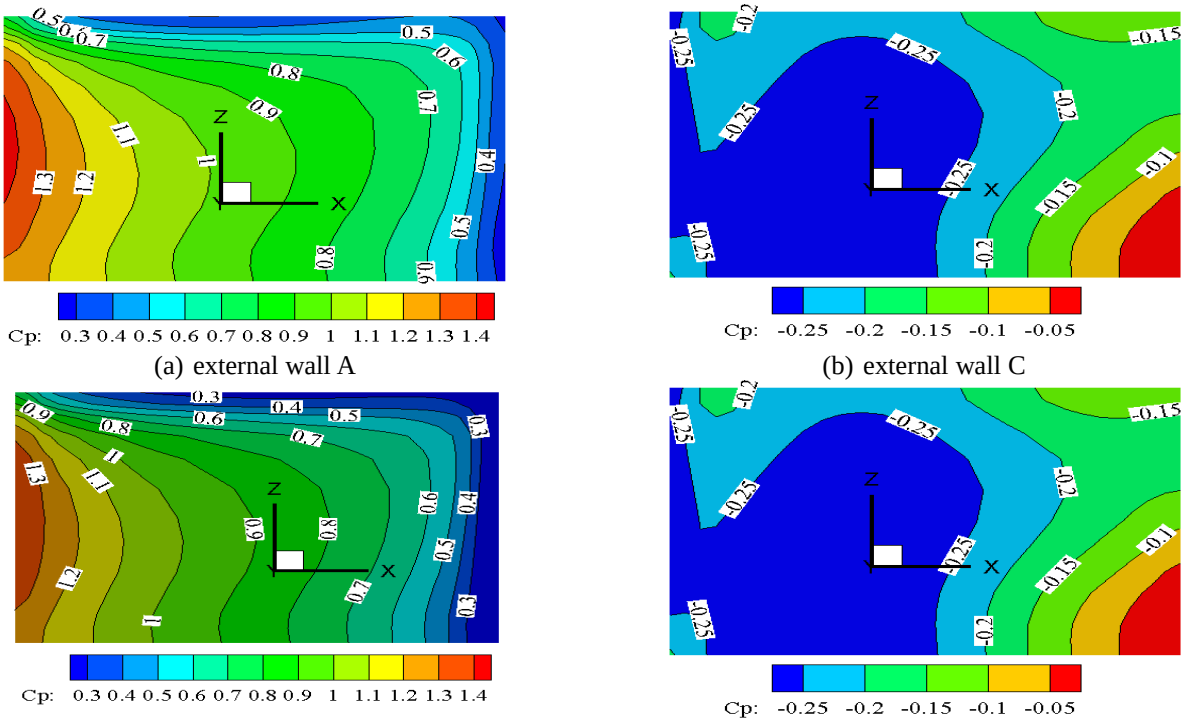

(a) external wall A (b) external wall C

(c) external wall B (d) external wall D

Fig. 21 Pressure coefficient distribution on external walls with wind attack angle 45°.

exhibit exactly same wind pressure coefficients, just as the external walls B and D in the case with wind attack angle 0°; see Fig. 16. Moreover, it is shown in Figs. 16 and 21 that compared with the case with wind attack angle 45°, the case with wind attack angle 0° exhibits a stronger wind suction effect on the external walls B and D and an almost wind push effect on external wall A. Therefore, the wind attack angle 0° is indeed the most unfavorable wind situation for rectangular buildings.

5. Conclusions

A full-scale measurement of wind field around the rectangular attic of a double-tower building is performed in this paper. Based on the measured data, the nature wind involving wind speed, temperature, turbulence intensity and turbulence integral length scale, and wind pressures are addressed. Power spectral densities, statistical histograms, spatial and temporal correlations of wind speed and wind pressures at measured points are analyzed. For a better understanding of wind pressure distribution on the attic facades, full-scale CFD simulations and comparative studies against the existing wind-load codes are carried out. Some concluding remarks are included as follows:

- Owing to the low mean wind speed and the large surface roughness length involved in the observation site, the turbulence intensity tends to be high and the turbulence integral length scale appears to be smaller.
- The wind velocity spectrum derived from the measured data shows a good consistency with the von Karman spectrum in both low and high frequency domains; and wind pressure spectra with respect to different measured points share a similar distribution despite the different wind conditions of them, which might be due to the effects of the main building on the wind field.
- Wind pressure coefficients distributed on the external walls of the rectangular attic arise to be of anisotropy along the horizontal and vertical directions, which are similar to the findings in previous experimental investigations of a square shape tall building by wind tunnel tests.
- Under the case with wind attack angle 0°, the wind pressure coefficients of the cross-wind facades expose remarkable variations along both horizontal and vertical directions; the wind pressure coefficients of the windward facade remain stable along horizontal direction but expose remarkable variations as well along vertical direction; while the variations of wind pressure coefficients of the leeward facades along both the horizontal and vertical directions can be safely ignored. The pattern of wind pressure coefficients, however, is not properly described in the existing wind-load codes.
- The wind attack angle 0° is the most unfavorable wind situation for rectangular buildings, which exhibits a strong wind suction effect on the crosswind facades and a remarkable wind push effect on the windward facade.

Acknowledgements

The financial supports from the National Key R&D Program of China (Grant No. 2017YFC0803300), the National Natural Science Foundation of China (Grant Nos. 51878505, 51725804 and 51538010) and the Ministry of Science and Technology of China (Grant No. SLDRCE19-B-26) are highly appreciated. The authors are grateful to Ms. Shifen Wang for her help in preparing the present paper.

References

Abdusemed, M.A. and Ahuja, A.K. (2016), "Effect of wind incidence angle on wind pressure distribution on square shape tall building", *Int. J. Res. Eng. Social Sci*., **6**(4), 45-52.

Ai, X.Q., Cheng, Y.Y. and Peng, Y.B. (2016), "Nonlinear dynamics and failure wind velocity analysis of urban trees", *Wind Struct*., **22**(1), 89-106. https://doi.org/10.12989/was.2016.22.1.089.

AIJ-RLB (2004), "*Recommandations on Loads for Buildings*", Architectural Institute of Japan, Tokyo: Japan, 19-22.

ASCE/SEI 7-10 (2010), "*Minimum Design Loads for Buildings and Other Structures*", American Society of Civil Engineers (ASCE), Reston: Virginia, 263-264.

Blocken, B. (2014), "50 years of Computational Wind Engineering: Past, present and future", *J. Wind Eng. Ind. Aerod*., **129**, 69-102. https://doi.org/10.1016/j.jweia.2014.03.008.

Blocken, B. and Carmeliet, J. (2008), "Pedestrian wind conditions at outdoor platforms in a high-rise apartment building: Generic sub-configuration validation, wind comfort assessment and uncertainty issues", *Wind Struct.*, **11**(1), 51-70. https://doi.org/10.12989/was.2008.11.1.051.

Blocken, B., Janssen, W.D. and van Hooff, T. (2012), "CFD simulation for pedestrian wind comfort and wind safety in urban areas: General decision framework and case study for the Eindhoven University campus", *Environ. Model. Softw.*, **30**, 15-34. https://doi.org/10.1016/j.envsoft.2011.11.009.

Blocken, B., Stathopoulos, T. and van Beeck, J.P.A.J. (2016), "Pedestrian-level wind conditions around buildings: Review of wind-tunnel and CFD techniques and their accuracy for wind comfort assessment", *Build. Environ.*, **100**, 50-81. https://doi.org/10.1016/j.buildenv.2016.02.004.

Clancy L.J. (1975), "*Aerodynamics*", Pitman Publishing Limited, London, England.

Davenport, A.G. (1961), "The spectrum of horizontal gustiness near the ground in high winds", *Q. J. R. Meteorol. Soc.*, **87**(372), 194-211. https://doi.org/10.1002/qj.49708737208.

EN 1991-1-4:2005(2005), "*Eurocode 1: Actions on Structures – Part 1-4 : General Actions – Wind Actions* "European Committee for Standardizaton(CEN), Brussels: Belgium, 34-37.

Franke J. (2006), "Recommendations of the COST action C14 on the use of CFD in predicting pedestrian wind environment", *Proceedings of the 4th International Symposium on Computational Wind Engineering (CWE2006)*, Yokohama Kanagawa.

Franke, J., Hellsten, A., Schlunzen, H. and Carissimo B. (2007), "*Best Practice Guideline for the CFD Simulation of Flows in the Urban Environment*", Quality Assurance and Improvement of Microscale Meteorological Models.

Fu, J.Y., Wu, J.R., Xu, A., Li, Q.S. and Xiao, Y.Q. (2012), "Full-scale measurements of wind effects on Guangzhou West Tower", *Eng. Struct.*, **35**, 120-139. https://doi.org/10.1016/j.engstruct.2011.10.022

GB50009-2012 (2012), "*Load Code for the Design of Building Structures*", The Ministry of Construction of China, Beijing: China, 45-47. (in Chinese).

Hu, L., Li, L. and Gu, M. (2010), "Error assessment for spectral representation method in wind velocity field simulation", *J. Eng. Mech.*, **136**(9), 1090-1104. https://doi.org/10.1061/(ASCE)EM.1943-7889.0000058.

Huang, S., Li, Q.S. and Xu, S. (2007), "Numerical evaluation of wind effects on a tall steel building by CFD", *J. Constr. Steel Res.*, **63**(5), 612-627. https://doi.org/10.1016/j.jcsr.2006.06.033.

Jendzelovsky, N., Antal, R. and Konecna, L. (2017), "Investigation of the external pressure coefficients on the facade of the triangular high-rise structure with curved corners", *Proceedings of the 3rd International Conference on Structural and Physical Aspects of Construction Engineering, SPACE 2016*. https://doi.org/10.1016/j.proeng.2017.05.355.

Kaimal, J.C., Wyngaard, J.C., Izumi, Y. and Coté, O.R. (1972), "Spectral characteristics of surface-layer turbulence", *Q. J. R. Meteorol. Soc.*, **98**(417), 563-589. https://doi.org/10.1002/qj.49709841707.

Kármán, T.v. (1948), "Progress in the statistical theory of turbulence", *Proceedings of the National Academy of Sciences*.

Ko, N.H., You, K.P. and Kim, Y.M. (2005), "The effect of non-Gaussian local wind pressures on a side face of a square building", *J. Wind Eng. Ind. Aerod.*, **93**(5), 383-397. https://doi.org/10.1016/j.jweia.2005.03.001.

Köse, D.A. and Dick, E. (2010), "Prediction of the pressure distribution on a cubical building with implicit LES", *J. Wind Eng. Ind. Aerod*., **98**(10-11), 628-649. https://doi.org/10.1016/j.jweia.2010.06.004.

Li, Q.S., Fang, J.Q., Jeary, A.P. and Wong, C.K. (1998), "Full scale measurements of wind effects on tall buildings", *J. Wind Eng. Ind. Aerod.*, 74-76 741-750. https://doi.org/10.1016/S0167-6105(98)00067-1.

Liu, Z.J., Liu, Z.H. and Peng, Y.B. (2018), "Simulation of multivariate stationary stochastic processes using dimension-reduction representation methods", *J. Sound Vib*., **418**, 144-162. https://doi.org/10.1016/j.jsv.2017.12.029.

Maruyama, T., Taniguchi, T., Okazaki, M. and Taniike, Y. (2008), "Field experiment measuring the approaching flows and pressures on a 2.4 m cube", *J. Wind Eng. Ind. Aerod.*, **96**(6-7), 1084-1091. https://doi.org/10.1016/j.jweia.2007.06.049.

Mittal, H., Sharma, A. and Gairola, A. (2018), "A review on the study of urban wind at the pedestrian level around buildings", *J. Build. Eng.*, **18**, 154-163. https://doi.org/10.1016/j.jobe.2018.03.006.

Montazeri, H. and Blocken, B. (2013), "CFD simulation of wind-induced pressure coefficients on buildings with and without balconies: Validation and sensitivity analysis", *Build. Environ.*, **60**, 137-149. https://doi.org/10.1016/j.buildenv.2012.11.012.

Peng, Y.B., Wang, S.F. and Li, J. (2018a), "Field measurement and investigation of spatial coherence for near-surface strong winds in Southeast China", *J. Wind Eng. Ind. Aerod*., **172**, 423-440. https://doi.org/10.1016/j.jweia.2017.11.012.

Peng, Y.B., Wang Z.H. and Ai, X.Q. (2018b), "Wind-induced fragility assessment of urban trees with structural uncertainties", *Wind Struct*., **26**(1), 45-56. https://doi.org/10.12989/was.2018.26.1.045.

Ren, G., Liu, J., Wan, J., Li, F., Guo, Y. and Yu, D. (2018), "The analysis of turbulence intensity based on wind speed data in onshore wind farms", *Renew. Energy.*, **123**, 756-766. https://doi.org/10.1016/j.renene.2018.02.080.

Richards, P.J. and Hoxey, R.P. (2012), "Pressures on a cubic building-Part 1: Full-scale results", *J. Wind Eng. Ind. Aerod.*, **102**, 72-86. https://doi.org/10.1016/j.jweia.2011.11.004.

Shinozuka, M. and Deodatis, G. (1996), "Simulation of multi-dimensional Gaussian stochastic fields by spectral representation", *Appl. Mech. Rev.*, **49**(1), 29-53.

Simiu, E. (1974), "Wind spectra and dynamic alongwind

response", *J. Struct. Div. - ASCE*, **100**(ST9, Paper 10815 (September, 1974)), 1897-1910.

Song, Y.P., Chen, J.B., Peng, Y.B., Spanos, P.D. and Li, J. (2018), "Simulation of nonhomogeneous fluctuating wind speed field in two-spatial dimensions via an evolutionary wavenumber-frequency joint power spectrum", *J. Wind Eng. Ind. Aerod.*, **179**, 250-259. https://doi.org/10.1016/j.jweia.2018.06.005

Tominaga, Y. (2015), "Flow around a high-rise building using steady and unsteady RANS CFD: Effect of large-scale fluctuations on the velocity statistics", *J. Wind Eng. Ind. Aerod.*, **142**, 93-103. https://doi.org/10.1016/j.jweia.2015.03.013.

Yan, Q., Peng, Y.B. and Li, J. (2013), "Scheme and application of phase delay spectrum towards spatial stochastic wind fields", *Wind Struct.*, **16**(5), 433-455. https://doi.org/10.12989/was.2013.16.5.433.

Zhao, L., Ge, Y. and Kareem, A. (2017), "Fluctuating wind pressure distribution around full-scale cooling towers", *J. Wind Eng. Ind. Aerod.*, **165**, 34-45. https://doi.org/10.1016/j.jweia.2017.02.016.

Zheng, C., Li, Y. and Wu, Y. (2016), "Pedestrian-level wind environment on outdoor platforms of a thousand-meter-scale megatall building: Sub-configuration experiment and wind comfort assessment", *Build. Environ.*, **106**, 313-326. https://doi.org/10.1016/j.buildenv.2016.07.004.

Zeng, X.S., Peng, Y.B. and Chen, J.B. (2017), "Serviceability-based damping optimization of randomly wind-excited high-rise buildings", *Strnct. Des. Tall Spec. Build.*, **26**(11), e1371. https://doi.org/10.1002/tal.1371.

CC